Mechanistic insights into the oxidation of copper(I) species during NH_3–SCR over Cu-CHA zeolites: A DFT study

Chong Liu,*[,†] Hiroe Kubota,[†] Takashi Toyao,[†,‡] Zen Maeno,[†] Ken-ichi Shimizu*[,†,‡]

[†] Institute for Catalysis, Hokkaido University, N-21, W-10, Sapporo 001-0021, Japan

[‡] Elements Strategy Initiative for Catalysts and Batteries, Kyoto University, Katsura, Kyoto 615-8520, Japan

Corresponding authors: chongliu@cat.hokudai.ac.jp (C.L.); kshimizu@cat.hokudai.ac.jp (K.S.)

Abstract

Selective catalytic reduction of nitrogen oxides using ammonia (NH_3–SCR) over Cu-exchanged zeolites proceeds via reduction of Cu(II) to Cu(I) and subsequent reoxidation of Cu(I) to Cu(II). Although the mechanism of reduction half cycle has been relatively well established, reoxidation pathways of Cu(I) to form the original Cu(II) species are highly complicated and remain unclear. Herein, oxidation mechanisms of Cu(I) to Cu(II) species in CHA zeolites during the NH_3–SCR process were investigated by periodic DFT calculations. The NH_3-solvated Cu(I) and Cu(II) species were considered for exploring the oxidative activation reaction pathways. The results show that, with O_2 as the sole oxidant, Cu(I) can be effectively oxidized to Cu(II) via multinuclear Cu-oxo intermediates with moderate reaction barriers. The NO-assisted oxidation of Cu(I) was found to favor the formation of Cu nitrate/nitrite species, which seem to only act as off-cycle resting states. We propose that reoxidation of Cu(I) to Cu(II) with O_2 as the sole oxidant plays a key role in the oxidation half cycle under standard NH_3–SCR conditions.

Keywords: NH_3–SCR, Cu-CHA zeolite, DFT calculation, multinuclear Cu species

1. Introduction

Selective catalytic reduction using ammonia (NH_3–SCR) is an efficient approach for converting harmful nitrogen oxides (NO_x) to nontoxic nitrogen and water molecules.[1–3] Small-pore Cu-exchanged chabazite zeolite (Cu-CHA) has recently attracted a lot of attention for its catalytic application in the NH_3–SCR due to the high activity and hydrothermal stability.[4–11] The stoichiometry of the standard SCR can be described in Eqn. (1).

$$2NO + 2NH_3 + 1/2O_2 \rightarrow 2N_2 + 3H_2O \quad (1)$$

It is generally believed that the standard NH_3–SCR over Cu-CHA catalysts is driven by the redox cycle of Cu(II)↔Cu(I).[12–18] The NH_3-solvated isolated Cu species have been suggested to play a key role in NH_3–SCR reaction.[13,19] On the basis of experimental and theoretical evidence,[13,20,21] the reduction half cycle accompanied by Cu(II) → Cu(I) reduction has been relatively well understood, which can be described in Eqn. (2) or (3), using the Cu(II) species in the form of $[Cu(NH_3)_3(OH)]^+$ or $[Cu(NH_3)_4]^{2+}$.

$$[Cu(NH_3)_3(OH)]^+ + NO \rightarrow [Cu(NH_3)_2]^+ + N_2 + 2H_2O \quad (2)$$

$$[Cu(NH_3)_4]^{2+} + NO \rightarrow [Cu(NH_3)_2]^+ + N_2 + H_2O + NH_4^+ \quad (3)$$

The $[Cu(NH_3)_3(OH)]^+$ represents the NH_3-solvated Cu(II) species exchanged to one $[AlO_2]^-$ site of the zeolite framework, which can be interconverted to Cu(II) species in the form of $[Cu(NH_3)_4]^{2+}$ by involving a Brønsted acid site (BAS) as described in Eqn. (4).

$$[Cu(NH_3)_3(OH)]^+ + NH_4^+ \rightarrow [Cu(NH_3)_4]^{2+} + H_2O \quad (4)$$

The exact speciation of Cu(II) may depend on the zeolite composition such as Si/Al and Cu/Al ratios as well as the reaction conditions.[15,22]

Although the reduction half cycle of NH_3–SCR over Cu-CHA has been relatively well explained, the mechanism for the oxidation half cycle accompanied by the activation of Cu(I) to Cu(II) remains in debate. DFT calculations suggest that direct O_2 dissociation on a single $[Cu(NH_3)_2]^+$ cluster does not occur.[23,24] Paolucci et al. proposed that the activation of O_2 proceeds via a dimeric Cu intermediate to accomplish the reoxidation process of Cu(I).[14,15] It was suggested that the NH_3-sovlated Cu(I) species, i.e., $[Cu(NH_3)_2]^+$, in Cu-CHA interact weakly with the zeolite framework, which can travel through zeolite windows to react with O_2 and yield an O-bridged Cu(II) dimer, as shown in Eqn. (5).[15] They assumed that NO is necessary for the decomposition of the Cu(II) dimer (Eqn. (6)). The reaction (6) can be divided into several elementary steps. DFT calculations show that NO promotes the decomposition of the $[Cu_2(\mu\text{-}O)_2(NH_3)_4]$ intermediate to produce Cu(II) nitrate species as described in Eqn. (7) .[14,23] Recently, Greenaway

et al.[25] have detected several key transient Cu intermediates including the Cu–NO_3 in the NH_3–SCR over Cu-CHA using the modulation excitation IR spectroscopy.

$$[Cu(NH_3)_2]^+ + 1/2O_2 \rightarrow 1/2[Cu_2(\mu\text{-}O)_2(NH_3)_4] \quad (5)$$

$$1/2[Cu_2(\mu\text{-}O)_2(NH_3)_4] + NO + 2NH_3 \rightarrow [Cu(NH_3)_3(OH)]^+ + N_2 + H_2O \quad (6)$$

$$[Cu_2(\mu\text{-}O)_2(NH_3)_4]^{2+} + NO \rightarrow [Cu(NO_3^-)(NH_3)_2]^+ + [Cu(NH_3)_2]^+ \quad (7)$$

It is believed that the nitrate ion (NO_3^-) on Cu(II) reacts with NO to yield gas-phase NO_2 and nitrite (NO_2^-) on Cu(II), which react with NH_3 (or NH_4^+) to afford N_2 and H_2O via the NH_4NO_2 intermediate, as shown in Eqns. (8) and (9).[26,27] A serious issue with the NO-assisted models in Eqns. (7)–(9) is the lack of supporting experimental evidence. In addition, computational study sufficiently describing each elementary step to recover the original Cu species has not been reported.

$$[Cu(NO_3^-)(NH_3)_2]^+ + NO \rightarrow [Cu(NO_2^-)(NH_3)_2]^+ + NO_2 \quad (8)$$

$$[Cu(NO_2^-)(NH_3)_2]^+ + 2NH_3 \rightarrow [Cu(NH_3)_3(OH)]^+ + N_2 + H_2O \quad (9)$$

Recently, we performed *in situ* spectroscopic experiments for Cu-CHA zeolites under steady-state NH_3–SCR conditions and transient conditions for Cu(II)/Cu(I) redox cycles, and the *in situ* XANES and UV-vis results suggest that the oxidation half cycle occurs with O_2 as the exclusive oxidant.[21] The *in situ* XANES experiments at 200 °C reported by Paolucci et al. also evidence that the $[Cu(NH_3)_2]^+$ complexes in CHA are oxidized by O_2 even in the absence of NO_x.[15] These experimental observations suggest that Cu(I) can be oxidized to Cu(II) by only O_2. However, the understanding of the detailed mechanism based on the spectroscopic experiments is difficult due to the limited information on the elementary steps.[21] In addition, NO-assisted oxidation is always coupled with consecutive reduction cycle, which makes it very challenging to design the transient experiments solely describing the distinguishable period of NO-assisted oxidation as well as the kinetics experiments for the comparison with O_2-only oxidation. In contrast, molecular-level study based on DFT calculations provides a plausible way to explore the detailed mechanism and to compare the reaction pathways of different oxidative activation modes.

Herein, we employed periodic DFT calculations to study the reaction mechanism for the reoxidation of Cu(I) to Cu(II) species in Cu-CHA zeolites. The reoxidation pathways by O_2 with and without NO assistance were investigated and compared. The key role of O_2 as the sole oxidant and the effect of NH_3 solvation during the oxidation half cycle of SCR reaction were emphasized.

2. Computational methods

Spin-polarized DFT calculations were carried out within periodic boundary conditions using the Vienna Ab initio Simulation Package (VASP).[28–30] The Perdew-Burke-Ernzerhof (PBE) functional[31] was used in combination with the projector augmented wave (PAW) method.[32,33] The cut-off energy of the plane waves was set to 500 eV. Brillouin zone sampling was restricted to the Γ point.[34] Van der Waals interactions were described by the dispersion-corrected DFT-D3 method with Becke-Johnson damping.[35] The convergence of the force on each atom was set to 0.05 eV $Å^{-1}$. The minimum-energy reaction pathway and the corresponding transition state (TS) were determined by the climbing image nudged elastic band (CI-NEB) method.[36] Such methodology settings have been successfully applied for studying various zeolite-catalyzed reactions including spin-polarized systems.[37–39] The minimum-energy reaction pathways were described using the energetics of the saddle points with their most stable spin states, and the detailed information on the spin transitions as well as the spin states of transition states and intermediates was summarized in the ESI (Table S1 and Fig. S1-S3).

Previous studies[12,13,23,40,41] showed that at low-temperature SCR conditions (e.g., 200 °C), the Cu ions in CHA zeolite are NH_3-solvated, which are detached from the zeolite framework as mobile species. It was suggested that Cu(I) ions diffuse in the form of linear $[Cu(NH_3)_2]^+$, which can readily pass through the eight-membered ring windows of the neighboring CHA cages. Here, such $[Cu(NH_3)_2]^+$ ions confined in a CHA cage were considered as the starting point for studying the oxidation mechanism of the SCR reaction. Zeolite CHA was modeled by a hexagonal unit cell ($Si_{36}O_{72}$),[42] and the initial Cu-containing model (Fig. 1) was built by introducing two $[Cu(NH_3)_2]^+$ ions and two Brønsted acid sites (BASs) in the CHA cage. Under NH_3–SCR conditions, the BASs exist in the form of NH_4^+ cations due to the strong adsorption of ammonia over H^+ sites,[21] and thus we considered NH_4^+ rather than bare H^+ as the relative sites for elementary steps involving the participation of BASs. Charge compensation for the cationic species was provided by the isomorphous substitution of Al^{3+} for lattice Si^{4+}, affording a Si/Al ratio of 8. Fully relaxed geometry optimizations were performed for all calculations with fixed lattice parameters ($a = b$ = 13.675 Å, c = 14.767 Å).[42]

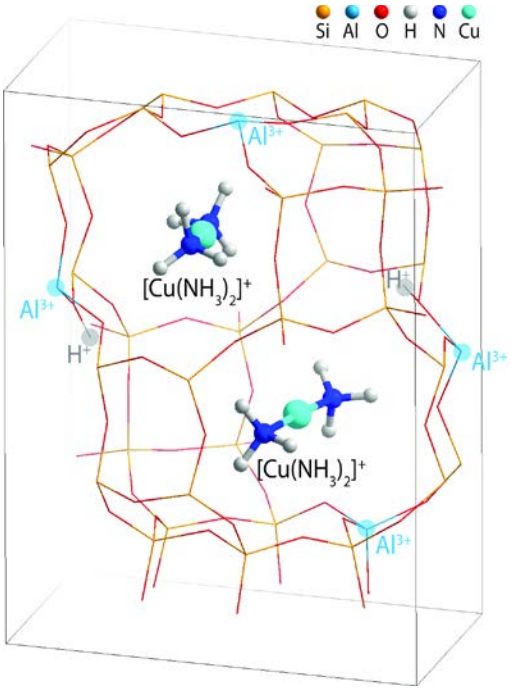

Fig. 1 Computational model of CHA unit cell with two $[Cu(NH_3)_2]^+$ cations and two Brønsted protons in the cage (36T, Si/Al=8).

3. Results and discussion

3.1 Reoxidation of Cu(I) by O_2

To verify the reoxidation mechanism without NO-assistance, the oxidation of Cu(I) to Cu(II) with O_2 as the sole oxidant were considered. The following stoichiometry can account for this process.

$$4[Cu(NH_3)_2]^+ + O_2 + 4NH_3 + 2H_2O \rightarrow 4[Cu(NH_3)_3(OH)]^+ \quad (10)$$

We first considered O_2 activation on a pair of $[Cu(NH_3)_2]^+$ as suggested in previous studies for Cu-CHA zeolites.[15,23] The dissociative activation of O_2 proceeds via two sequential elementary steps with computed activation barriers of 20 and 13 kJ/mol, and the system energy is decreased by −63 kJ/mol (Fig. 2). A dimeric $[Cu_2(\mu\text{-}O)_2]^{2+}$ species is formed after O_2 dissociative activation.

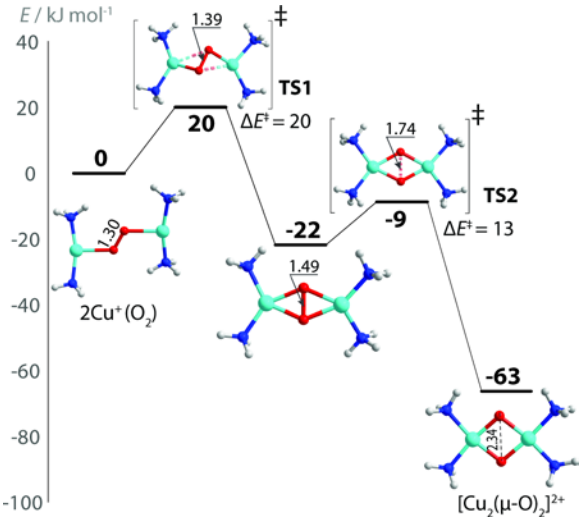

Fig. 2 Energy profiles for O_2 dissociation and oxidation of two mononuclear $[Cu(NH_3)_2]^+$. Zeolite frameworks are omitted for clarity. Atomic distances are given in Å.

As the stoichiometric chemistry requires the transfer of four electrons for exclusive O_2 activation, two additional $[Cu(NH_3)_2]^+$ ions were introduced in the CHA cage. The presence of an extra pair of $[Cu(NH_3)_2]^+$ around the dimeric $[Cu_2(\mu\text{-}O)_2]^{2+}$ leads to the formation of a tetranuclear $[Cu_4(\mu_3\text{-}O)_2]^{4+}$ cluster where each μ-O site binds to three Cu ion centers, and the computed reaction barriers are 44 and 31 kJ/mol for the sequential coordination of the two $[Cu(NH_3)_2]^+$ with the bridging oxygens in $[Cu_2(\mu\text{-}O)_2]^{2+}$ (Fig. 3). The decomposition of the tetranuclear $[Cu_4(\mu_3\text{-}O)_2]^{4+}$ occurs via the consecutive hydrolysis of Cu–O bonds and produces two dicopper $[Cu_2(\mu\text{-}OH)(\eta\text{-}OH)]^{2+}$ sites, which act as precursors for the production of oxidized mononuclear Cu^{2+} species (Fig. 4). The two consecutive hydrolysis reactions have activation barriers of 81 and 79 kJ/mol, respectively. The produced dicopper $[Cu_2(\mu\text{-}OH)(\mu\text{-}OH)]^{2+}$ intermediates can readily decompose into $[Cu(OH)]^+$ ions with a low activation barrier of 48 kJ/mol (Fig. 5a). The further

dehydration reaction of $[Cu(OH)]^+$ and a Brønsted proton (in the form of NH_4^+) to afford Cu^{2+} ions only requires a barrier of 50 kJ/mol (Fig. 5b). For the oxidation of Cu(I) to Cu(II) by O_2 as an exclusive oxidant, the highest activation barrier of ca. 81 kJ/mol was found for the hydrolysis reactions during the decomposition of the tetranuclear $[Cu_4(\mu_3\text{-}O)_2]^{4+}$ cluster.

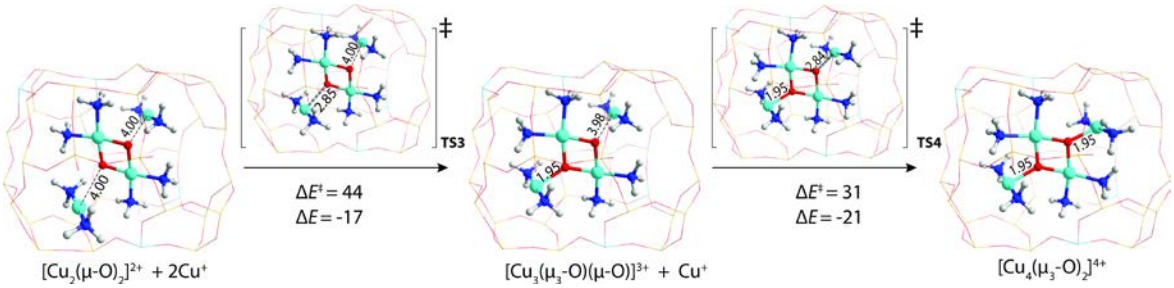

Fig. 3 Formation of tetranuclear $[Cu_4(\mu_3\text{-}O)_2]^{4+}$ via the reaction of dimeric $[Cu_2(\mu\text{-}O)_2]^{2+}$ and an extra pair of $[Cu(NH_3)_2]^+$ confined in one CHA cage. Activation and reaction energies ($\Delta E^{\ddagger}$ and ΔE) are given in kJ/mol. Cu–O distances are indicated in Å.

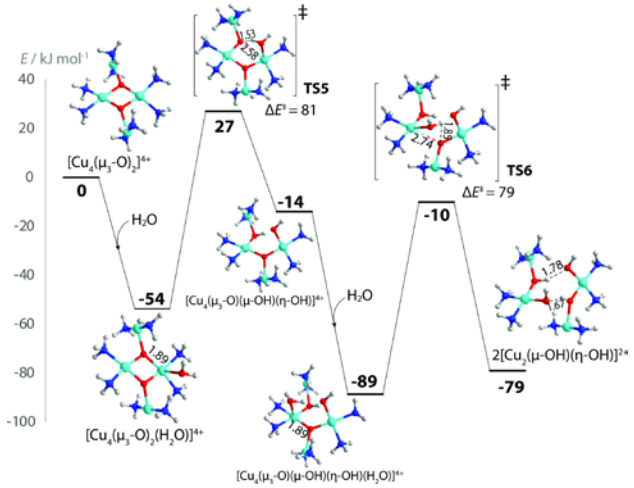

Fig. 4 Energy profiles for the H_2O-assisted decomposition of a tetranuclear $[Cu_4(\mu_3\text{-}O)_2]^{4+}$ into two dicopper $[Cu_2(\mu\text{-}OH)(\eta\text{-}OH)]^{2+}$ sites. Zeolite frameworks are omitted for clarity. Atomic distances are given in Å.

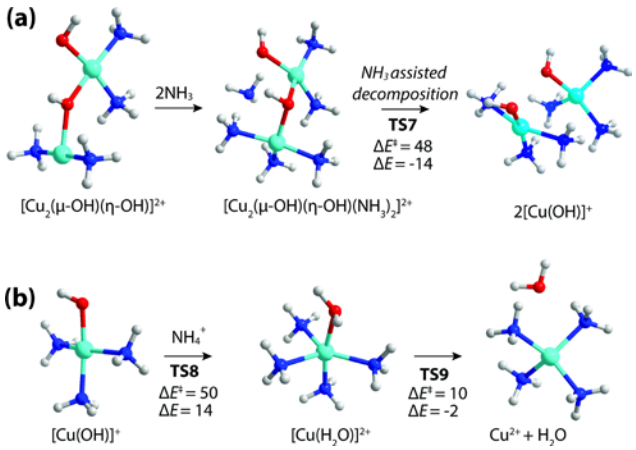

Fig. 5 (a) NH_3 assisted decomposition of dicopper $[Cu_2(\mu\text{-}OH)(\eta\text{-}OH)]^{2+}$ into two $[Cu(OH)]^+$ ions; (b) Formation of Cu^{2+} species from the dehydration reaction of $[Cu(OH)]^+$ and a Brønsted proton (in the form of NH_4^+). Activation and reaction energies ($\Delta E^{\ddagger}$ and ΔE) are in kJ/mol. Zeolite frameworks are omitted for clarity.

Due to the limited spectral resolution, it is difficult to distinguish the exact nuclearity of Cu-oxo clusters in CHA zeolites from the experimental spectroscopic characterizations.[21] The present theoretical results show that the formation of the Cu tetramer from a dimeric $[Cu_2(\mu\text{-}O)_2]^{2+}$ and a pair of $[Cu(NH_3)_2]^+$ is energetically favorable (Fig. 3). The driving force for this process is related to the basicity of bridging oxygens in Cu-oxo dimer and the unsaturated coordination of $[Cu(NH_3)_2]^+$ cations.[37] It should be noted that such a Cu tetramer model corresponds to the situation when NH_3-solvated Cu(I) is sufficiently supplied, and therefore it is more appropriate for the description of zeolite samples with high Cu loadings. If Cu(I) cations in zeolite matrix are sufficiently diluted, the formation of such Cu tetranuclear species will be very unlikely.

To validate the reoxidation process in Cu-zeolites with less sufficient Cu loadings, we also considered the reaction pathway via the direct decomposition of $[Cu_2(\mu\text{-}O)_2]^{2+}$, as generated from the O_2 dissociation on two $[Cu(NH_3)_2]^+$ clusters (Fig. 2). The two consecutive H_2O dissociations on $[Cu_2(\mu\text{-}O)_2]^{2+}$ require reaction barriers of 85 and 88 kJ/mol (Fig. 6a), which are slightly higher than the case of the Cu tetramer model (81 and 79 kJ/mol). The hydrolysis reactions produce two mononuclear $[Cu(OH)_2]^+$ intermediates, which show similar Cu oxidation states as the original dimeric $[Cu_2(\mu\text{-}O)_2]^{2+}$. To satisfy the stoichiometry of this process (Eqn. (10)), the $[Cu(OH)_2]^+$ intermediate is necessary to react with another Cu(I) species, i.e., $[Cu(NH_3)_2]^+$. The coordination of the hydroxyl groups in $[Cu(OH)_2]^+$ to the $[Cu(NH_3)_2]^+$ generates a $[Cu_2(\mu\text{-}OH)_2]^{2+}$ intermediate with a reaction barrier of 33 kJ/mol (Fig. 6b). It was found that the direct decomposition of $[Cu_2(\mu\text{-}OH)_2]^{2+}$ into two three-coordinated Cu(II) sites is difficult, and the coordination of additional NH_3 molecules to the Cu centers is necessary, which stabilizes the target

$[Cu(OH)]^+$ sites in square planar geometries. Such a stabilization effect of NH_3 ligands suggests the important role of NH_3 solvation during the conversions of Cu complexes under NH_3–SCR conditions.

The reoxidation of Cu(I) species can be realized via the H_2O-assisted decomposition of $[Cu_2(\mu\text{-}O)_2]^{2+}$ or $[Cu_4(\mu_3\text{-}O)_2]^{4+}$. Although the exact elementary steps are different, the above discussed two types of O_2-only reoxidations require similar activation barriers and gives the same final stoichiometry as described in Eqn. (10). The highest barriers were found for the hydrolysis reactions of Cu–O bonds in the multinuclear Cu-oxo intermediates with estimated barriers of 81–88 kJ/mol. We believe that, depending on the catalyst composition, reaction conditions, etc., the nuclearity of the multinuclear Cu-oxo intermediates may change. As the formation of multinuclear Cu-oxo intermediates is necessary, a higher Cu loading in zeolite matrix will be beneficial for such activations. This is consistent with previous experimental studies describing that the reoxidation half cycle becomes faster when higher amount of Cu is loaded in the zeolite.[14,15,21]

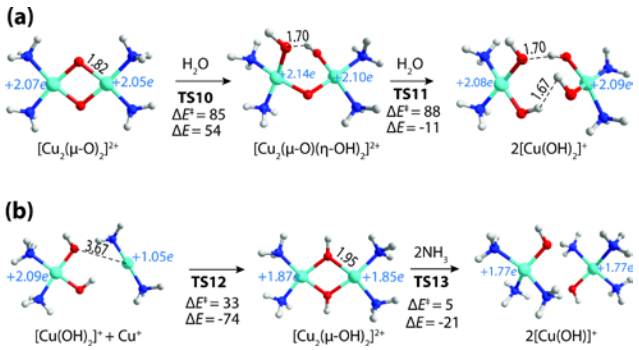

Fig. 6 (a) H_2O-assisted decomposition of a dimeric $[Cu_2(\mu\text{-}O)_2]^{2+}$ into two mononuclear $[Cu(OH)_2]^+$ intermediates; (b) NH_3 solvation assisted formation of two $[Cu(OH)]^+$ sites from the reaction of $[Cu(OH)_2]^+$ and Cu(I) ions. Zeolite frameworks are omitted for clarity. Atomic distances are given in Å. The Bader charges of Cu are normalized with reference to the bulk CuO (+2.00 *e*).

3.2 Reoxidation of Cu(I) by NO + O_2

The oxidation of Cu(I) by O_2 assisted by NO can also afford Cu(II) species. Gao et al.[14] suggested that this process proceeds with the $[Cu^+\text{-}O_2\text{-}Cu^+]$ intermediate followed by the reaction of NO to form the $[Cu^+(\mu\text{-}O)Cu^+(NO_2)]^{2+}$. The desorption of NO_2 gives $[Cu_2(\mu\text{-}O)]^{2+}$, which can further be hydrolyzed into two $[Cu(OH)]^+$. For this process, NO_2 formation was found to be the rate-determining step with a free activation energy of 104 kJ/mol. Chen et al.[23] later found that NO oxidation via the $[Cu_2(\mu\text{-}O)_2]^{2+}$ intermediate requires an activation barrier of 42 kJ/mol. Here, we also considered this mechanism for NO_2 formation (Fig. 7), and a similar barrier of 46 kJ/mol was obtained for the formation of the $[Cu^+(\mu\text{-}O)Cu^+(NO_2)]^{2+}$ intermediate.

To form the $[Cu_2(\mu\text{-}O)]^{2+}$ intermediate, which is a precursor for producing NO_x-ligand-free $[Cu(OH)]^+$ or Cu^{2+}, the bound NO_2 in $[Cu^+(\mu\text{-}O)Cu^+(NO_2)]^{2+}$ needs to be released from the Cu center.[14] This process was found unfavorable by 74 kJ/mol with an estimated barrier of 90 kJ/mol. In contrast, the further oxidation of NO_2 in $[Cu^+(\mu\text{-}O)Cu^+(NO_2)]^{2+}$ to yield the $[Cu(NO_3)]^+$ species only requires an activation barrier of 51 kJ/mol with an exothermicity of −78 kJ/mol, implying a strong preference for further NO_2 oxidation to nitrate species. This is consistent with the previous theoretical studies showing the adsorption of NO promotes the dissociation of O_2 and the production of Cu nitrate species.[23,24] In Ref. 23, it was shown that the activation of NO and O_2 on a single Cu(I) complex can also produce Cu(II) nitrate ($Cu^+ + NO + O_2 \rightarrow [Cu(NO_3)]^+$), and the computed activation barrier of 78 kJ/mol is higher than the situation when the nitrate species is formed on a pair of complexes. The role of such nitrate species in the SCR process is still unclear and controversial;[43–45] they possibly act as off-cycle resting states or even show a poisoning effect if NH_4NO_3 acts as a major side product.[46] Understanding the further conversion of the nitrate species to recover the original Cu species is key to explain their role in SCR reaction, but the corresponding elementary steps have not been fully explored yet.

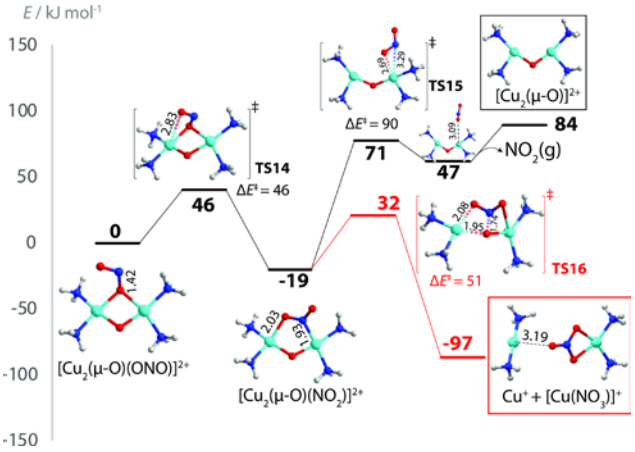

Fig. 7 Energy profile for the NO-assisted activation of Cu(I) into Cu(II) species in CHA zeolite. Zeolite frameworks are omitted for clarity. Atomic distances are given in Å.

To release the Cu^{2+} or $[Cu(OH)]^+$ cations, which act as active sites to convert NO and NH_3 into N_2 in the reduction half cycle ($Cu^{2+} + NO + NH_3 \rightarrow Cu^+ + H^+ + N_2 + H_2O$; $[Cu(OH)]^+ + NO + NH_3 \rightarrow Cu^+ + N_2 + 2H_2O$),[13,15] the Cu(II) nitrate and nitrite species are necessarily converted into NO_x-ligand-free cations to close the full SCR cycle. Therefore, the possible conversion paths of such nitrate and nitrite species were explored. The direct formation of NO_x-ligand-free Cu(II) from nitrate species by reacting with Brønsted acid protons was first studied. Except the Cu nitrate in chelating bidentate configuration with two NH_3 ligands as described in Fig. 7, the possible structures of Cu nitrates with three NH_3 ligands proposed by Negri et al.[45] and the corresponding structurally analogous Cu nitrite were also considered (Fig. S4). TS calculations suggested the release of nitrate/nitrite moieties from Cu centers requires activation barriers of

146–225 kJ/mol, which are considerably higher than the estimated barriers (81–88 kJ/mol) required in the reoxidation process by O_2 as a sole oxidant.

In the presence of NO, the nitrate $[Cu(NO_3)]^+$ can be reduced back to nitrite $[Cu(NO_2)]^+$ by simultaneous oxidation of NO into NO_2 (Fig. 8a). This process was found to occur via a stepwise mechanism, similar to that reported by Chen et al.[23] The release of a NO_3 unit from the Cu nitrate species forms a $[Cu(NO_3NO)]^+$ intermediate with a partially reduced Cu center, which further proceeds to a $[Cu(NO_2)]^+$ and a neutral NO_2 molecule. For such a process, the forward and backward elementary steps only require a maximum barrier of 47 kJ/mol, implying the possible fast interconversion between Cu nitrate and nitrite species at typical SCR temperatures (e.g., 200 °C). In addition, the preadsorbed NO_2 in the zeolite pores was found to easily oxidize Cu^+ into the form of $[Cu(NO_2)]^+$ without a barrier (Fig. 8b, $Cu^+ + NO_2 \rightarrow$ Nitrite), and this process is highly exothermic by −97 kJ/mol. The NO_2-monodentated nitrite $[Cu(NO_2)]^+$ can also be transformed into its NO_2-bidentated form $[Cu(\eta^2\text{-}NO_2)]^+$ (Fig. 8b, Nitrite → $[Cu(\eta^2\text{-}NO_2)]^+$), requiring a barrier of 48 kJ/mol with an endothermicity of 12 kJ/mol. To obtain the target products of N_2 and H_2O, it is generally believed that the formation of highly unstable intermediates is necessary, which can be either nitrosamine intermediate (NH_2NO) or ammonium nitrite (NH_4NO_2).[46] We then evaluated the production of such intermediates from Cu nitrite species. The intramolecular reaction of $[Cu(NO_2)]^+$ with a NH_3 ligand to form the $[Cu(OH)(NH_2NO)]^+$ intermediate (Fig. 8b, Nitrite → $[Cu(OH)(NH_2NO)]^+$) destabilizes the system by 164 kJ/mol. Similarly, the intermolecular reaction of $[Cu(NO_2)]^+$ and a Brønsted proton (in the form of NH_4^+) to release a Cu^{2+} and a neutral NH_4NO_2 unit (Fig. 8b, Nitrite → $Cu^{2+} + NH_4NO_2$) is highly endothermic by 225 kJ/mol. Even if the reaction of $[Cu(NO_2)]^+$ and NH_4^+ is assumed to form a water molecule to compensate the system energy (Fig. 8b, Nitrite → $[Cu(NH_2NO)]^{2+} + H_2O$), the transformation is still unfavorable by 129 kJ/mol with reference to the initial state of the nitrite species. Due to the high stability of Cu-bound nitrite and nitrate species,[47] their conversion to highly unstable NH_2NO or NH_4NO_2 intermediates is strongly inhibited and therefore very unlikely to occur under standard SCR conditions at typical working temperatures (e.g., 200 °C). In comparison with the oxidation of Cu(I) by O_2 as an exclusive oxidant where NO_x-ligand-free cupric cations are directly produced (Scheme S1), the NO-involved oxidation yields highly stable nitrate/nitrate species, and their further conversion to release Cu^{2+} or $[Cu(OH)]^+$ cations is needed to close the full SCR cycle (Scheme S2). However, such necessary conversions are strongly inhibited by thermodynamics due to the highly stable nature of nitrate/nitrite species, and thus they seem more likely to act as off-cycle resting states, which play a minor role in the standard SCR reaction. This conclusion is consistent with recent experimental studies using transient FTIR spectroscopy[43] and time-resolved X-ray absorption spectroscopy (XAS),[48] which suggest that nitrates are not involved in the SCR process under typical low-temperature conditions. Based on the experimental[21,43,48] and current theoretical results, we propose that in the redox reaction of the SCR process, the main

contribution to the oxidation of Cu(I) to Cu(II) is from the exclusive O_2 oxidation rather than the NO-assisted oxidation process.

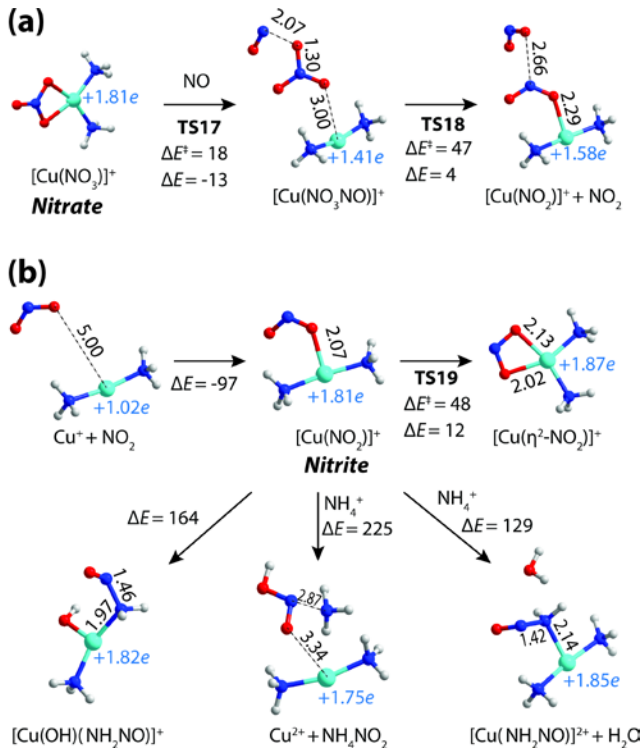

Fig. 8 Reaction pathways for the conversion of cationic cupric (a) nitrate and (b) nitrite species in CHA cage. Zeolite frameworks are omitted for clarity. Activation and reaction energies ($\Delta E^{\ddagger}$ and ΔE) are given in kJ/mol. The Bader charges of Cu are normalized with reference to the bulk CuO (+2.00 *e*).

Under standard NH_3–SCR conditions, the reoxidation of Cu(I) by only O_2 competes with the NO-assisted reoxidation. The presence of NO will affect both the NO-assisted reoxidation and the NO-participated reduction half cycle. For the exclusive O_2 oxidation, the produced Cu(II) species will react with NO and NH_3 as described in Eqn. (2) or (3), which undergoes the reduction half cycle to produce N_2, and the consumption of Cu(II) species will drive the whole catalytic cycle (Scheme S1). In this case, the formation of N_2 in SCR process is mainly contributed from the reduction cycle, which is consistent with our previous experiments[21] showing that the transient rate of N_2 formation in the reduction half cycle is close to the steady-state SCR rate. In contrast, the catalytic cycle driven by NO-assisted reoxidation is inhibited by the conversion of nitrate/nitrite species to N_2 (Scheme S2), which more likely plays a minor contribution in low temperature NH_3–SCR reaction.

3.3 Effect of Hubbard corrections

Finally, we evaluated the effect of Hubbard corrections on the energetics of key reaction steps during Cu(I) oxidations. Chen et al.[49] recently employed different exchange–correlation functionals to study the same O_2 activation process on a pair of $[Cu(NH_3)_2]^+$ in Cu-CHA zeolite, and the reported activation barriers for the first transition state is ranged from 20 to 46 kJ/mol, suggesting the choice of functionals can affect the potential energy curves. By the comparison with the experimental results of copper oxide references, they suggested the correct description of Cu–O bonds are only achieved by the functional with a Hubbard-U term. Thus, we also considered the Hubbard term corrections for the activation and reaction energies ($\Delta E^{\ddagger}$ and ΔE) of selected key reactions (Table 1). The U-parameter for Cu 3d was set to 6 eV,[49,50] and the transition states and intermediates were re-optimized with a Hubbard term (PBE+D+U). The comparison suggests that the Hubbard-U corrections do not afford significant changes of $\Delta E^{\ddagger}$ and ΔE for the selected reaction step. This is possibly because the method errors for a given type of structures are often similar.[51] For the oxidation of Cu(I) by O_2 without NO assistance, the Hubbard-U corrected $\Delta E^{\ddagger}$ for the hydrolysis reactions of Cu–O bonds, as the most difficult steps in the O_2-only oxidation process, are 84–88 k/mol. In contrast, the necessary reaction steps in NO + O_2 oxidation, i.e, the formation of NH_2NO or NH_4NO_2, are much more energetically unfavorable (126–226 k/mol). Therefore, the consideration of Hubbard term correction does not affect our conclusion on the major role of exclusive O_2 activation in the NH_3–SCR reaction.

Table 1 Energetics of selected reaction steps with and without Hubbard-U corrections. Activation and reaction energies ($\Delta E^{\ddagger}$ and ΔE) are given in kJ/mol

Reaction step	PBE+D		PBE+D+U	
	$\Delta E^{\ddagger}$	ΔE	$\Delta E^{\ddagger}$	ΔE
$[Cu_2(\mu\text{-}O)_2]^{2+} + H_2O \rightarrow [Cu_2(\mu\text{-}O)(\eta\text{-}OH)_2]^{2+}$ (Fig. 6a, TS10)	85	54	88	62
$[Cu_2(\mu\text{-}O)(\eta\text{-}OH)_2]^{2+} + H_2O \rightarrow 2[Cu(OH)_2]^{+}$ (Fig. 6a, TS11)	88	-11	84	-13
Nitrite $\rightarrow [Cu(OH)(NH_2NO)]^{+}$ (Fig. 8b)		164		163
Nitrite $\rightarrow Cu^{2+} + NH_4NO_2$ (Fig. 8b)		225		226
Nitrite $\rightarrow [Cu(NH_2NO)]^{2+} + H_2O$ (Fig. 8b)		129		126

4. Conclusions

To summarize, the reaction mechanism of the oxidation half cycle of NH_3–SCR over Cu-CHA zeolites was studied by periodic DFT calculations. The NH_3-sovated Cu(I) species, i.e., $[Cu(NH_3)_2]^+$, were employed as the starting point, and the oxidative activations of such species to Cu(II) species in the form of $[Cu(NH_3)_4]^{2+}$ or $[Cu(OH)(NH_3)_3]^+$ were considered. The results show that Cu(I) species are oxidized by O_2 to generate multinuclear Cu-oxo intermediates such as $[Cu_2(\mu\text{-}O)_2]^{2+}$ or $[Cu_4(\mu_3\text{-}O)_2]^{4+}$. The further decomposition of these Cu-oxo clusters proceeds via sequential hydrolysis reactions of Cu–O bonds and the effect of NH_3 solvation, which produces the original Cu(II) species as active sites for the next reduction half cycle. Such oxidation processes with O_2 as the exclusive oxidant require moderate reaction barriers of ca. 81–88 kJ/mol. The NO-assisted oxidation was found to favor the formation of Cu(II) nitrate/nitrite species. These nitrate/nitrite species show high stability, which inhibits their further conversion to N_2 and H_2O as target products, and thus act more likely as off-cycle resting states. We propose that the oxidation of Cu(I) to Cu(II) species by O_2 as the exclusive oxidant plays a major role in the standard NH_3–SCR reaction.

Conflicts of interest

There are no conflicts to declare.

ACKNOWLEDGEMENT

This research is one of the projects promoted by the research association of Automotive Internal Combustion Engines (AICE) and financially supported by Japan Ministry of Economy, Trade and Industry and auto industries. Also, this work was financially supported by the JST-CREST project JPMJCR17J3, KAKENHI grants 17H01341, 18K14057, and 18K14051 from JSPS, and by MEXT projects “Elements Strategy Initiative to Form Core Research Centers” and IRCCS. C.L. acknowledges the JSPS postdoctoral fellowship (No. P19059). Part of the calculations were performed on supercomputers at RIIT (Kyushu Univ.) and ACCMS (Kyoto Univ.).

REFERENCES

1 A. M. Beale, F. Gao, I. Lezcano-Gonzalez, C. H. F. Peden and J. Szanyi, *Chem. Soc. Rev.*, 2015, **44**, 7371–7405.

2 R. Zhang, N. Liu, Z. Lei and B. Chen, *Chem. Rev.*, 2016, **116**, 3658–3721.

3 S. V. Priya, T. Ohnishi, Y. Shimada, Y. Kubota, T. Masuda, Y. Nakasaka, M. Matsukata, K. Itabashi, T. Okubo, T. Sano, N. Tsunoji, T. Yokoi and M. Ogura, *Bull. Chem. Soc. Jpn.*, 2018, **91**, 355–361.

4 J. H. Kwak, R. G. Tonkyn, D. H. Kim, J. Szanyi and C. H. F. Peden, *J. Catal.*, 2010, **275**, 187–190.

5 J. S. McEwen, T. Anggara, W. F. Schneider, V. F. Kispersky, J. T. Miller, W. N. Delgass and F. H. Ribeiro, *Catal. Today*, 2012, **184**, 129–144.

6 Y. Xin, Q. Li and Z. Zhang, *ChemCatChem*, 2018, **10**, 29–41.

7 Y. Jangjou, Q. Do, Y. Gu, L. G. Lim, H. Sun, D. Wang, A. Kumar, J. Li, L. C. Grabow and W. S. Epling, *ACS Catal.*, 2018, **8**, 1325–1337.

8 T. Usui, Z. Liu, S. Ibe, J. Zhu, C. Anand, H. Igarashi, N. Onaya, Y. Sasaki, Y. Shiramata, T. Kusamoto and T. Wakihara, *ACS Catal.*, 2018, **8**, 9165–9173.

9 Y. J. Kim, P. S. Kim and C. H. Kim, *Appl. Catal., A*, 2019, **569**, 175–180.

10 X. Auvray, A. Grant, B. Lundberg and L. Olsson, *Catal. Sci. Technol.*, 2019, **9**, 2152–2162.

11 Y. Shan, X. Shi, G. He, K. Liu, Z. Yan, Y. Yu and H. He, *J. Phys. Chem. C*, 2018, **122**, 25948−25953.

12 T. V. W. Janssens, H. Falsig, L. F. Lundegaard, P. N. R. Vennestrøm, S. B. Rasmussen, P. G. Moses, F. Giordanino, E. Borfecchia, K. A. Lomachenko, C. Lamberti, S. Bordiga, A. Godiksen, S. Mossin and P. Beato, *ACS Catal.*, 2015, **5**, 2832–2845.

13 C. Paolucci, A. A. Parekh, I. Khurana, J. R. Di Iorio, H. Li, J. D. Albarracin Caballero, A. J. Shih, T. Anggara, W. N. Delgass, J. T. Miller, F. H. Ribeiro, R. Gounder and W. F. Schneider, *J. Am. Chem. Soc.*, 2016, **138**, 6028–48.

14 F. Gao, D. Mei, Y. Wang, J. Szanyi and C. H. F. Peden, *J. Am. Chem. Soc.*, 2017, **139**, 4935–4942.

15 C. Paolucci, I. Khurana, A. A. Parekh, S. Li, A. J. Shih, H. Li, J. R. Di Iorio, J. D. Albarracin-Caballero, A. Yezerets, J. T. Miller, W. N. Delgass, F. H. Ribeiro, W. F. Schneider and R. Gounder, *Science*, 2017, **357**, 898–903.

16 G. E. Douberly, A. M. Ricks, P. V. R. Schleyer and M. A. Duncan, *J. Phys. Chem. A*, 2008, **112**, 4869–4874.

17 C. Paolucci, A. A. Verma, S. A. Bates, V. F. Kispersky, J. T. Miller, R. Gounder, W. N. Delgass, F. H. Ribeiro and W. F. Schneider, *Angew. Chem. Int. Ed.*, 2014, **53**, 11828–11833.

18 Y. Li, J. Deng, W. Song, J. Liu, Z. Zhao, M. Gao, Y. Wei and L. Zhao, *J. Phys. Chem. C*, 2016, **120**, 14669–14680.

19 R. Zhang and J. S. McEwen, *J. Phys. Chem. Lett.*, 2018, **9**, 3035–3042.

20 A. Godiksen, O. L. Isaksen, S. B. Rasmussen, P. N. R. Vennestrøm and S. Mossin, *ChemCatChem*, 2018, **10**, 366–370.

21 C. Liu, H. Kubota, T. Amada, K. Kon, T. Toyao, Z. Maeno, K. Ueda, J. Ohyama, A. Satsuma, T. Tanigawa, N. Tsunoji, T. Sano and K. Shimizu, *ChemCatChem*, 2020, DOI:10.1002/cctc.202000024.

22 B. Kerkeni, D. Berthout, D. Berthomieu, D. E. Doronkin, M. Casapu, J. D. Grunwaldt and C. Chizallet, *J. Phys. Chem. C*, 2018, **122**, 16741–16755.

23 L. Chen, H. Falsig, T. V. W. Janssens and H. Grönbeck, *J. Catal.*, 2018, **358**, 179–186.

24 H. Falsig, P. N. R. Vennestrøm, P. G. Moses and T. V. W. Janssens, *Top. Catal.*, 2016, **59**, 861–865.

25 A. G. Greenaway, A. Marberger, A. Thetford, I. Lezcano-González, M. Agote-Arán, M. Nachtegaal, D. Ferri, O. Kröcher, C. R. A. Catlow and A. M. Beale, *Chem. Sci.*, 2020, **11**, 447–455.

26 D. Wang, L. Zhang, K. Kamasamudram and W. S. Epling, *ACS Catal.*, 2013, **3**, 871–881.

27 C. Tyrsted, E. Borfecchia, G. Berlier, K. A. Lomachenko, C. Lamberti, S. Bordiga, P. N. R. Vennestrøm, T. V. W. Janssens, H. Falsig, P. Beato and A. Puig-Molina, *Catal. Sci. Technol.*, 2016,

6, 8314–8324.
28 G. Kresse and J. Hafner, *Phys. Rev. B*, 1993, **48**, 13115–13118.
29 G. Kresse and J. Hafner, *Phys. Rev. B*, 1994, **49**, 14251–14269.
30 G. Kresse and J. Furthmüller, *Phys. Rev. B*, 1996, **54**, 11169–11186.
31 J. P. Perdew, K. Burke and M. Ernzerhof, *Phys. Rev. Lett.*, 1996, **77**, 3865–3868.
32 P. E. Blöchl, *Phys. Rev. B*, 1994, **50**, 17953–17979.
33 D. Kresse, G.; Joubert, *Phys. Rev. B*, 1999, **59**, 1758–1775.
34 H. J. Monkhorst and J. D. Pack, *Phys. Rev. B*, 1976, **13**, 5188–5192.
35 S. Grimme, S. Ehrlich and L. Goerigk, *J. Comput. Chem.*, 2011, **32**, 1456–1465.
36 G. Henkelman and H. Jónsson, *J. Chem. Phys.*, 2000, **113**, 9978–9985.
37 E. A. Pidko, E. J. M. Hensen and R. A. Van Santen, *Proc. R. Soc. A*, 2012, **468**, 2070–2086.
38 G. Li, P. Vassilev, M. Sanchez-Sanchez, J. A. A. Lercher, E. J. M. J. M. Hensen and E. A. A. Pidko, *J. Catal.*, 2016, **338**, 305–312.
39 C. Liu, G. Li and E. A. Pidko, *Small Methods*, 2018, **2**, 1800266.
40 F. Giordanino, E. Borfecchia, K. A. Lomachenko, A. Lazzarini, G. Agostini, E. Gallo, A. V. Soldatov, P. Beato, S. Bordiga and C. Lamberti, *J. Phys. Chem. Lett.*, 2014, **5**, 1552–1559.
41 K. A. Lomachenko, E. Borfecchia, C. Negri, G. Berlier, C. Lamberti, P. Beato, H. Falsig and S. Bordiga, *J. Am. Chem. Soc.*, 2016, **138**, 12025–12028.
42 L. J. Smith, A. Davidson and A. K. Cheetham, *Catal. Letters*, 1997, **49**, 143–146.
43 Y. Zhang, Y. Peng, K. Li, S. Liu, J. Chen, J. Li, F. Gao and C. H. F. Peden, *ACS Catal.*, 2019, 6137–6145.
44 C. Negri, P. S. Hammershøi, T. V. W. Janssens, P. Beato, G. Berlier and S. Bordiga, *Chem. Eur. J.*, 2018, **24**, 12044–12053.
45 C. Negri, E. Borfecchia, M. Cutini, K. A. Lomachenko, T. V. W. Janssens, G. Berlier and S. Bordiga, *ChemCatChem*, 2019, **11**, 3828–3838.
46 F. Gao and C. H. F. Peden, *Catalysts*, 2018, **8**, 140.
47 T. Anggara, C. Paolucci and W. F. Schneider, *J. Phys. Chem. C*, 2016, **120**, 27934–27943.
48 A. Marberger, A. W. Petrov, P. Steiger, M. Elsener, O. Kröcher, M. Nachtegaal and D. Ferri, *Nat. Catal.*, 2018, **1**, 221–227.
49 L. Chen, T. V. W. Janssens and H. Grönbeck, *Phys. Chem. Chem. Phys.*, 2019, **21**, 10923–10930.
50 L. Y. Isseroff and E. A. Carter, *Phys. Rev. B*, 2012, **85**, 235142.
51 T. J. Goncalves, P. N. Plessow and F. Studt, *ChemCatChem*, 2019, **11**, 4368–4376.